Supplementary Materials

Manipulating the orientations of the electric and magnetic dipoles induced in silicon nanoparticles for multicolor display

Jin Xiang,[1#] Juntao Li,[2#] Zhenpeng Zhou,[2] Shuai Jiang,[1] Jindong Chen,[1] Qiaofeng Dai,[1] Shaolong Tie,[3] Sheng Lan,[1]* and Xuehua Wang[2]*

[1]*Guangdong Provincial Key Laboratory of Nanophotonic Functional Materials and Devices, School of Information and Optoelectronic Science and Engineering, South China Normal University, Guangzhou 510006, China*

[2]*State Key Laboratory of Optoelectronic Materials and Technologies, Sun Yat-Sen University, Guangzhou, 510275, China*

[3]*School of Chemistry and Environment, South China Normal University, Guangzhou 510006, China*

*Corresponding author: slan@scnu.edu.cn; wangxueh@mail.sysu.edu.cn

[#]Authors contributed equally to this work.

Table of contents

1. Orientations of the ED and MD induced in a Si nanosphere

In Fig. S1, we show the electric and magnetic field distributions on the XZ and YZ planes calculated at the electric and magnetic dipole (ED and MD) resonances of a Si nanosphere (NS) with a diameter of $d = 187$ nm. The Si NS is illuminated by using a plane wave propagating along the z direction and polarized along the x direction. It can be seen clearly that an ED and a MD, which orients along the x and y direction respectively, are induced in the Si NS. In this case, the ED and MD resonances appear simultaneously in the forward scattering spectrum of the Si NS, which is detected in the z direction. As a result, the scattering light appears as white.
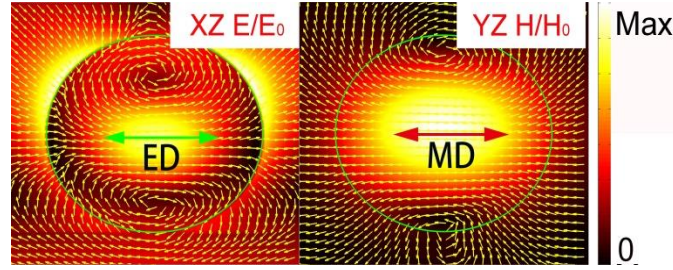

Figure S1: Electric and magnetic field distributions showing the ED and MD induced in a Si NS with $d = 187$ nm. The Si NS is illuminated with a plane wave propagating along the z direction and polarized along the x direction.

2. Electric and magnetic fields of the evanescent wave in total internal reflection

For the total internal reflection occurring at the interface between glass/quartz (with refractive index of n_1) and air (with refractive index of n_2), which is shown in Fig. S2, we can write:

$$\begin{cases} k_{1x} = k_1 \sin \varphi \\ k_{1z} = k_1 \cos \varphi \\ k_{1y} = 0 \end{cases} \text{ and } k_2^2 = k_{2x}^2 + k_{2z}^2 .$$ Here, k_1 and k_2 are the wave vectors of the incident and transmitted light, φ_1 and φ' are the incidence and refraction angles. According to the continuity boundary condition, we have $k_{1x}^r = k_{2x} = k_{1x}$ and $k_1 \sin \varphi = k_2 \sin \varphi'$, where k_1^r is the wave vector of the reflected light. Based on the Snell equation, we have $n_1 \sin \varphi = n_2 \sin \varphi'$ and $k_2 = k_1 n$, where $n = n_2 / n_1$. Thus, one can obtain the x and z components of k_2, which are expressed as:

$$k_{2x} = k_{1x} = k_1 \sin \varphi, \quad k_{2z} = \sqrt{k_2^2 - k_{2x}^2} = k_1 \sqrt{n^2 - \sin \varphi^2} .$$

For s-polarized light, we can derive the electric field of the evanescent wave which is given by $\mathbf{E}' = \mathbf{y} E_0' e^{-\beta z} e^{i(k_{2x}x - \omega t)}$, where $\beta = k_1 \sqrt{\sin^2 \varphi - n^2}$. According to Maxwell equations

2

$\nabla \times \mathbf{E}_0 = i k_0 \sqrt{\mu_0 / \varepsilon_0} \mathbf{H}_0$, the magnetic field of the evanescent wave is deduced to be

$\mathbf{H}' = \dfrac{1}{\mu \omega} E_0' e^{-\beta z} e^{i(k_{2x}x - \omega t)} (-\mathrm{i}\beta\mathbf{x} + k_{2x}\mathbf{z})$. The same method can be employed to derive the electric and

magnetic fields of the evanescent wave for *p*-polarized light which are expressed as follows:

$\mathbf{E}_p' = E_0' e^{-\beta z} e^{i(k_{2x}x - \omega t)} (-\mathrm{i}\dfrac{\beta}{k_0}\mathbf{x} + \dfrac{k_{2x}}{k_0}\mathbf{z})$, $\mathbf{H}_p' = \mathbf{y} E_0' \sqrt{\varepsilon_0 / \mu_0} e^{-\beta z} e^{i(k_{2x}x - \omega t)}$.
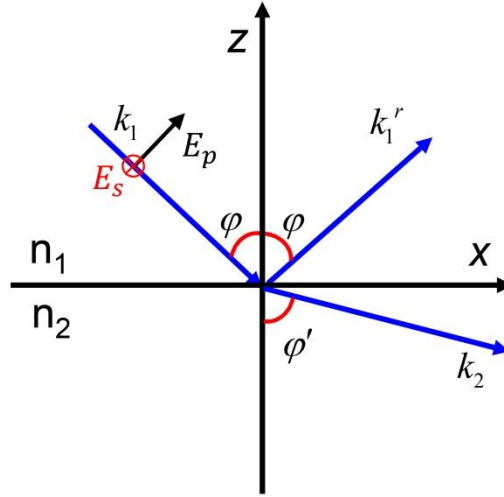

Figure S2: Total internal reflection occurring at the interface between glass/quartz (n_1) and air (n_2).

3. Field enhancement in evanescent wave excitation

In Fig. S3, we show the magnetic and electric distributions along the normal of the glass substrate calculated for *p*- and *s*-polarized light at two incidence angles of $\varphi = 33°$ and 43°, respectively. For $\varphi = 33°$ which is close to the incidence angle in the conventional dark-field microscopy, the enhancement factors derived for the magnetic and electric fields are found to be ~1.5. In comparison, larger enhancement factors for the magnetic field (~3.0) and electric field (~2.0) are observed on the surface of the glass substrate for $\varphi = 43°$ at which the total internal reflection occurs. It implies that an enhanced scattering intensity is expected for Si nanoparticles which are excited by using the evanescent wave generated in a total internal reflection configuration, as described in this work.
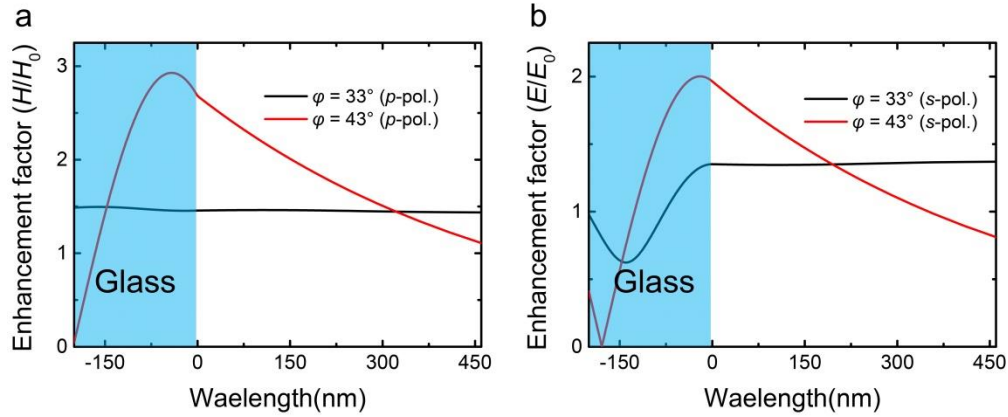
Figure S3: (a) Magnetic field distributions ($|H/H_0|$) along the normal of the glass slide when the prism is excited by *p*-polarized light at an incidence angle smaller ($\varphi = 33°$) or equal to the critical angle ($\varphi = 43°$) for total internal reflection. (b) Electric field distributions ($|E/E_0|$) along the normal of the glass slide when the prism is excited by *s*-polarized light at an incidence angle smaller ($\varphi = 33°$) or equal to the critical angle ($\varphi = 43°$) for total internal reflection.

4. Influence of the substrate on the scattering properties of Si nanoparticles

We have examined the influence of a glass/quartz substrate with a refractive index of ~1.45 on the scattering properties of Si nanoparticles. In Fig. S4a, the scattering spectra of a Si NS with a diameter of d = 186 nm were calculated without and with a glass substrate. It can be seen that the existence of the glass substrate leads to a slight broadening of the ED and MD resonances. A comparison of the scattering spectra calculated for a Si nanopillar (NP) (with a diameter of d = 130 nm and a height of h = 150 nm) without and with a quartz substrate is shown in Fig. S4b. Similarly, a slight broadening of the ED and MD resonances is observed for the Si NP in the presence of the quartz substrate. These results indicate that the influence of a glass/quartz substrate on the scattering properies and structural colors of Si nanoparticles can be neglected because of their low refractive index.

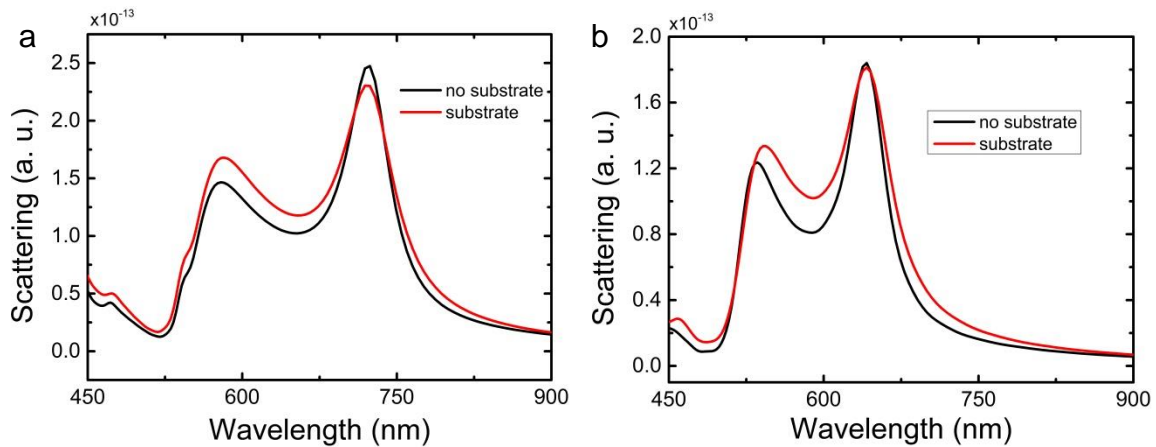

Figure S4: (a) Scattering spectra calculated for a Si NS with d = 186 nm without and with a glass substrate. (b) Scattering spectra calculated for a Si NP with d = 130 nm and h = 150 nm without and with a quartz substrate.

5. Decomposition of the scattering spectrum of a Si nanosphere

The scattering spectrum of a Si NS excited by using a plane wave propagating in the z direction can be decomposed into the contributions of EDs and MDs oriented in different directions, i.e., p_x, p_y, p_z, m_x, m_y, and m_z by using the multipole expansion method, as shown in Fig. S5. It can be seen that the total scattering of the Si NS originates from p_y and m_x, which are induced by the electric and magnetic fields of the incident light. As compared with the Si NS excited by using the evanescent wave (see Fig. 2c in the main text), the scattering intensities of the MD and ED resonances of the Si NS excited by using the plane wave are much weaker.
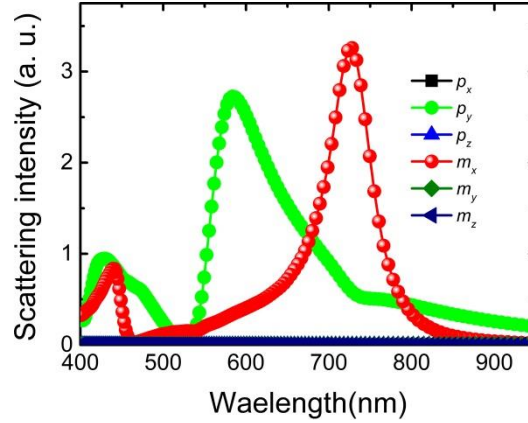

Figure S5: Decomposition of the scattering spectrum of a Si NS with $d = 187$ nm, which is excited by using a plane wave, into the contributions of EDs and MDs oriented in different directions by using multipolar expansion.

6. Derivation of the color indices from the scattering spectra of Si nanoparticles

Based on the theory of colorimetry, the color of an object can be described by its tristimulus values (X, Y, and Z) which are related with the chromaticity coordinates (x, y, and z) by the following equations:

$$X = k \int S(\lambda)\bar{x}(\lambda)\beta(\lambda)d\lambda$$
$$Y = k \int S(\lambda)\bar{y}(\lambda)\beta(\lambda)d\lambda \tag{1}$$
$$Z = k \int S(\lambda)\bar{z}(\lambda)\beta(\lambda)d\lambda$$

$$x = X / Y + Y + Z$$
$$y = Y / X + Y + Z \tag{2}$$
$$z = Z / X + Y + Z$$

Here, $S(\lambda)$ is the relative power of the illumination at wavelength λ, $\bar{x}(\lambda)$, $\bar{y}(\lambda)$, and $\bar{z}(\lambda)$ are the color matching functions for the CIE 1931 2 °Standard Observer, $\beta(\lambda)$ is the spectral reflectivity of the sample at wavelength λ.

Similar to the use of the reflection spectrum of an object to derive the color index of the object, the color index of the scattering light of a Si nanoparticle can also be derived based on the scattering spectrum of the Si nanoparticle. A typical example is shown in Fig. S6.
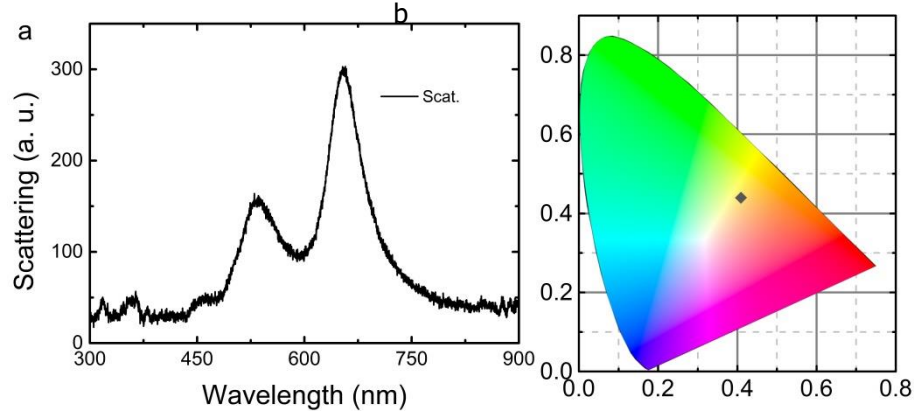

Figure S6: (a) Scattering spectrum measured for a Si NS with d ~ xxx nm. (b) Color index derived from the scattering spectrum of the Si NS based on Eq. (1). The chromaticity coordinates were calculated to be $x = 0.414$, $y = 0.431$, and $z = 0.155$.

7. Influence of the incidence angle on the scattering spectrum of a Si nanosphere

As discussed in the main text, the excitation of a Si NS by using the evanescent wave generated in the total internal reflection configuration is equivalent to that by using both the incident and reflected light with a fixed phase difference. The calculated dependence of the phase difference on the incidence angle is shown in the inset of Fig. 2a. At the critical angle, it can be seen that the incident and reflected light are in phase for both *s*- and *p*-polarized light. The phase difference becomes larger at larger incidence angles. In Fig. S7a, we show the evolution of the scattering spectrum with increasing incidence angle for *s*- and *p*-polarized light. For *p*-polarized light, it is noticed that the scattering intensity of the MD increases while that of the ED decreases when the incidence angle is increased. The situation is reversed for *s*-polarized light. In order to confirm this feature, we measured the scattering spectra of a Si NS with $d = 170$ nm which are excited by *p*- and *s*-polarized light at different incidence angles of 45°, 50°, and 55°, as shown in Fig. S7b. When the incidence angle was increased from 45° to 55°, a slight increase of the ED resonance was observed for *p*-polarized light while a slight increase of the MD resonance was observed for *s*-polarized. From Fig. S7, it can be seen that a significant increase in the ED/MD resonance is observed only at incidence angles larger than 60°. Therefore, the slight change of the incidence angle around the critical value does not influence so much the scattering spectrum and thus the scattering light color.
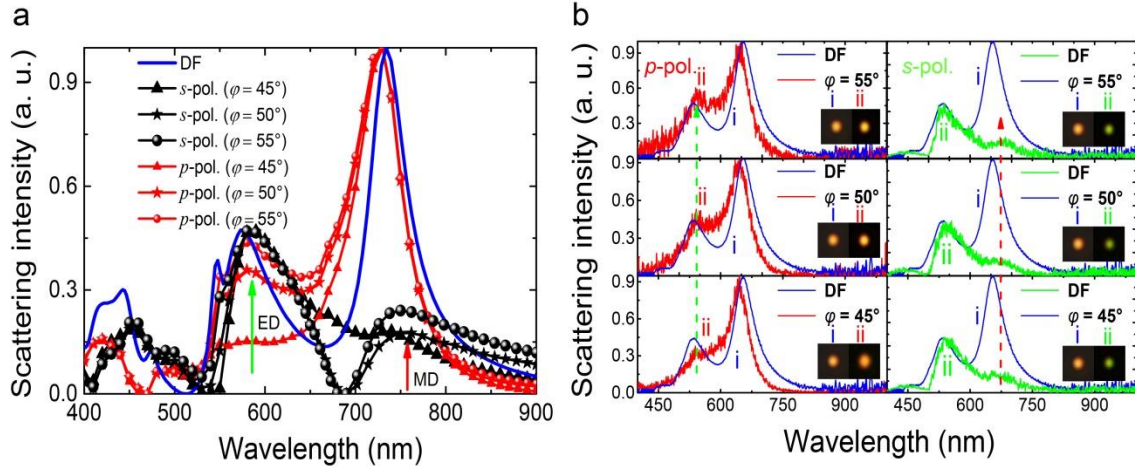
Figure S7: (a) Evolution of the ED and MD resonances in the scattering spectrum with increasing incidence angle above the critical value calculated for *s*- and *p*-polarized light. (b) Scattering spectra of a Si NS with *d* = 170 nm excited by *p*- and *s*-polarized light at different incidence angles. The scattering spectrum of the Si NS measured by using a dark-field microscope is also provided for comparison. In each case, the scattering light recorded by using a CCD is shown in the inset.

8. Scattering spectra calculated for Si nanopillars excited by evanescent waves

We have simulated the scattering spectra of Si NPs with a fixed height of *h* = 130 and different diameters excited by using *p*-, *s*-, and a plane wave, as shown in Fig. S8.
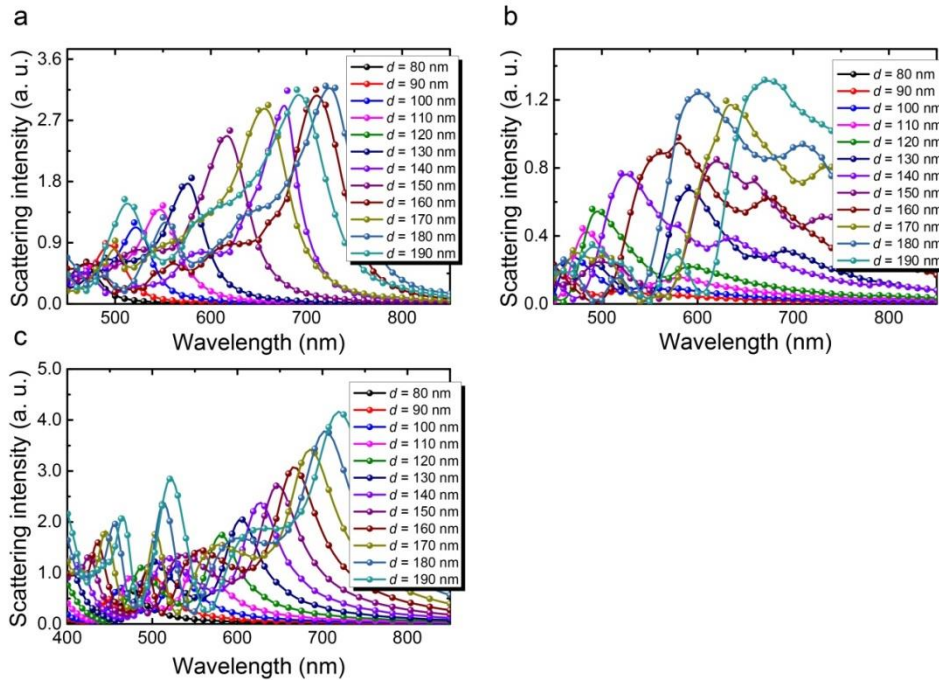

Figure S8: Scattering spectra calculated for Si NPs with a fixed height of *h* = 130 nm and different diameters excited by using *p*-polarized light (a), *s*-polarized light (b), and a plane wave (c).

9. Color display of the regular arrays of Si nanopillars

In Fig. S9, we show the appearance of a Si-based metasurface composed of Si NPs with four different diameters of d_1 = 142 nm, d_2 = 105 nm, d_3 = 150 nm, and d_4 = 119 nm. The detailed structure of the metasurface can be found in the main text. We illuminated the metasurface in different modes and recorded the appearances of the metasurface. In the case of normal incidence, no distinct color can be observed because of the simultaneous excitation of the ED and MD resonances, as shown in Figs. S9a and S9b. Under the dark-field microscope, one can see different colors because the relative intensities of the ED and MD resonances have been changed by the oblique incident light, as shown in Figs. S9c and S9d. However, the chromaticity and the background noise are not satisfied. In the case of evanescent wave excitation, the chromaticity is improved significantly and the background noise is reduced considerably, as shown in Fig. S9e.
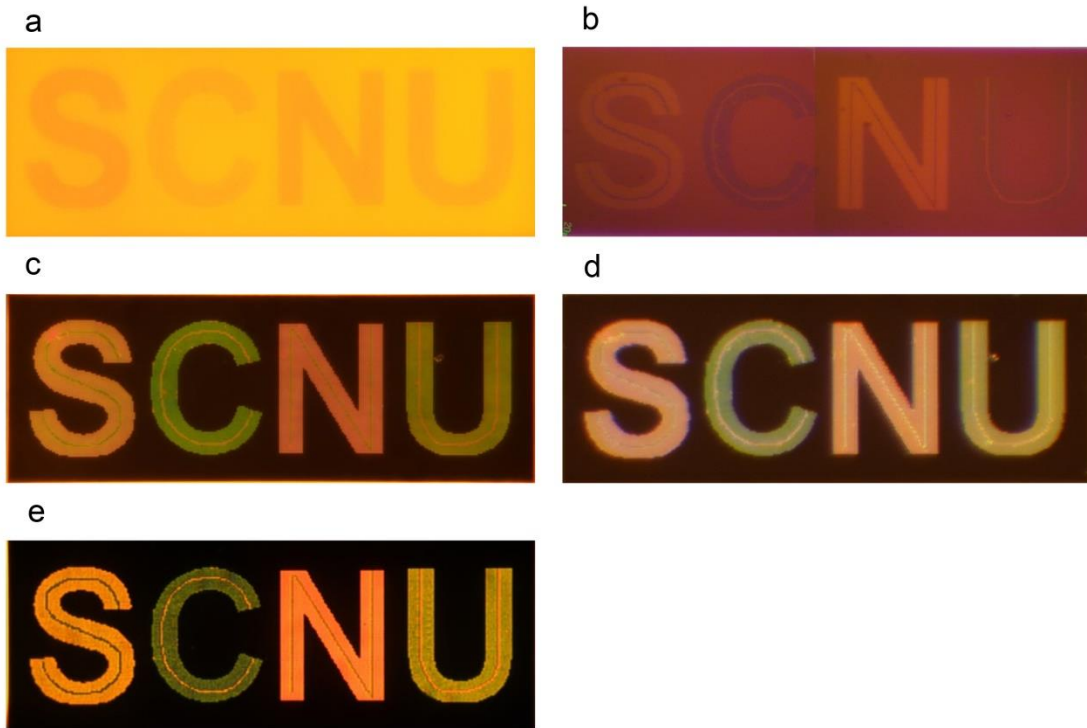

Figure S9: Regular array of Si NPs illuminated in different modes. (a) Transmission of the array recorded by using a 60× objective. (b) Reflection of the array recorded by using a 60× objective. (c) Dark-field transmission of the array recorded by using a 100× objective. (d) Dark-field reflection of the array recorded by using a 50× objective. (e) Evanescence wave excitation of the array with un-polarized light.

10. Arrays of Si nanopillars with a large period of 800 nm

In Fig. S10a, we show the CCD image of a regular array of Si NPs with a fixed height of h = 130 nm and different diameters. The Si NPs are regularly arranged on a square lattice with a period of p = 800 nm. The scattering light from single Si NPs can be clearly identified. The SEM image of the letter "U" is shown in Fig. 10Sb. From the magnified image shown in the inset, one can see the difference in the diameter of Si NPs.
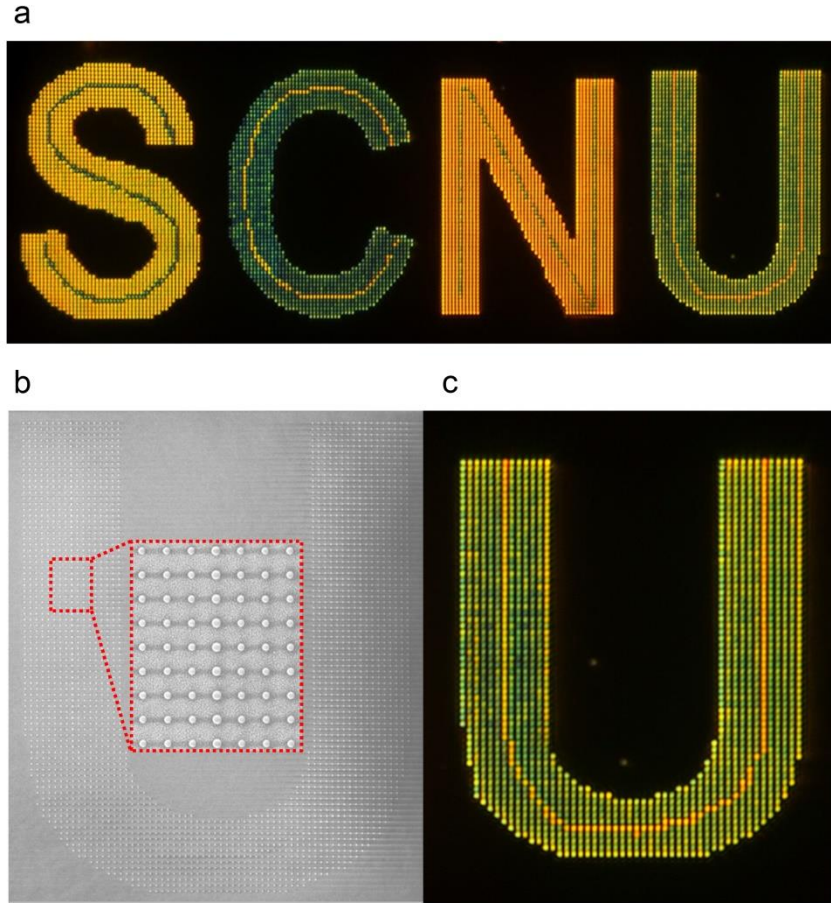

Figure S10: (a) CCD image of the array of Si NPs with a fixed height of h = 130 nm and different diameters. The pitch of the array was p = 800 nm. (b) SEM image of the letter "U" showing the constituent Si NPs. (c) Magnified CCD images of the letter "U".

11. Influence of the height of a Si nanopillar on the scattering spectrum

For regular arrays of Si NPs, the height of the constituent Si NPs is usually chosen to be h = 220 nm, which is the thickness of the conventional SIO wafer. However, the evanescent wave generated in the total internal reflection configuration decays rapidly along the z direction and Si NPs with such a height may not be effectively excited, leading to a broadened scattering spectrum, as shown in Fig. S11a. In this case, the tunable range of the scattering light color is narrow. In Fig. S11b, we show the scattering

spectrum of a Si NP with a reduced height of h = 150 nm. It can be seen that both the ED and MD resonances become narrower under the excitation of s- and p-polarized light. If the height of the Si NPs can be further reduced to h = 130 nm, then the tunable range of the scattering light color obtained by using Si NPs is comparable to that achieved by using Si NSs.
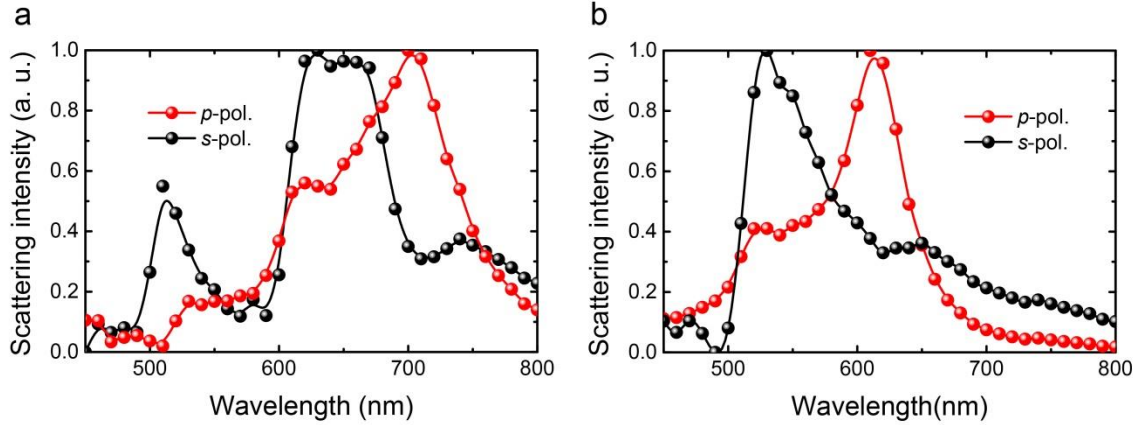

Figure S11: Scattering spectra calculated for a Si NP with the same diamter (d = 130 nm) and different heights of h = 220 nm (a) and h = 150 nm (b) under the excittaion of s- and p-polarized light.

12. Spatial resolution of the multicolor display based on the regular arrays of Si nanopillars

We have examined by numerical simulation the influence of coupling between Si NPs on the scattering properties and structural colors. In Fig. S12a, we present the scattering spectra calculated for a 3 × 3 array of Si NPs with a period of p = 500 nm excited by using s- and p-polarized light. The scattering spectra calculated for a single Si NP is also provided for comparison. It can be seen that the coupling between Si NPs can be neglected when the period of the array is chosen to be p = 500 nm. Also, we have considered the influence of the surrounding Si NPs on the scattering properties of the Si NPs in the central line, which is the situation shown in Fig. 5 of the main text. For simplicity, we simulated the scattering spectra of a 3 × 3 array composed of Si NPs with different diameters of d = 100 and 130 nm, as shown in the inset of Fig. S12b. The simulated scattering spectra for two periods of p = 800 and 500 nm are presented in Figs. S12b and S12c, respectively. In the numerical simulations, the detector used to record the scattering intensity of the Si NPs in the central line was placed just above the Si NPs (the blue rectangle) so that only the scattering light from the Si NPs in the central line was collected. For p = 800 nm, it can be seen that the scattering spectra are modified only slightly when comparing the scattering spectra of a single Si NP. It implies that the existence of the surrounding Si NPs with d = 130 nm has negligible influence on the scattering light color exhibited by the Si NPs in the central line (d = 130 nm). When the period of the array is reduced to p = 500 nm, however, a significant change in the scattering spectra is observed, as shown in Fig. S12c. The dashed circles in Fig. S12c indicate the original scattering

peaks of the Si NPs in the central line ($d = 110$ nm) without the surrounding Si NPs ($d = 130$ nm). It means that the visual appearance of the Si NPs in the central line has been strongly influenced by the neighboring Si NPs, as indicated by the reviewer. In Fig. S12d, we present the scattering spectra simulated for the Si NPs with $d = 100$ and 130 nm. It can be seen that the scattering intensity of the Si NPs with $d = 130$ nm is much stronger than that of the Si NPs with $d = 100$ nm. When the large Si NPs ($d = 130$ nm) are brought close to the small ones ($d = 100$ nm), the scattering spectra of the small Si NPs will be dramatically changed and the original scattering peaks appear as small shoulders in the modified spectra (see Fig. S12d). As a result, the visual appearance of the central line deviates significantly from the designed structural color. Actually, the simulation results described above are in good with the experimental observations. In Figs. 5(c)-5(e) of the main text, the structural color of the central line in letter "S" was designed to be green. However, the visual appearance of the central light is not green because of the small period of $p = 500$ nm of the array. When the period is increased to $p = 800$ nm, the structural color of the central line is close to the designed one (see Fig. S10).
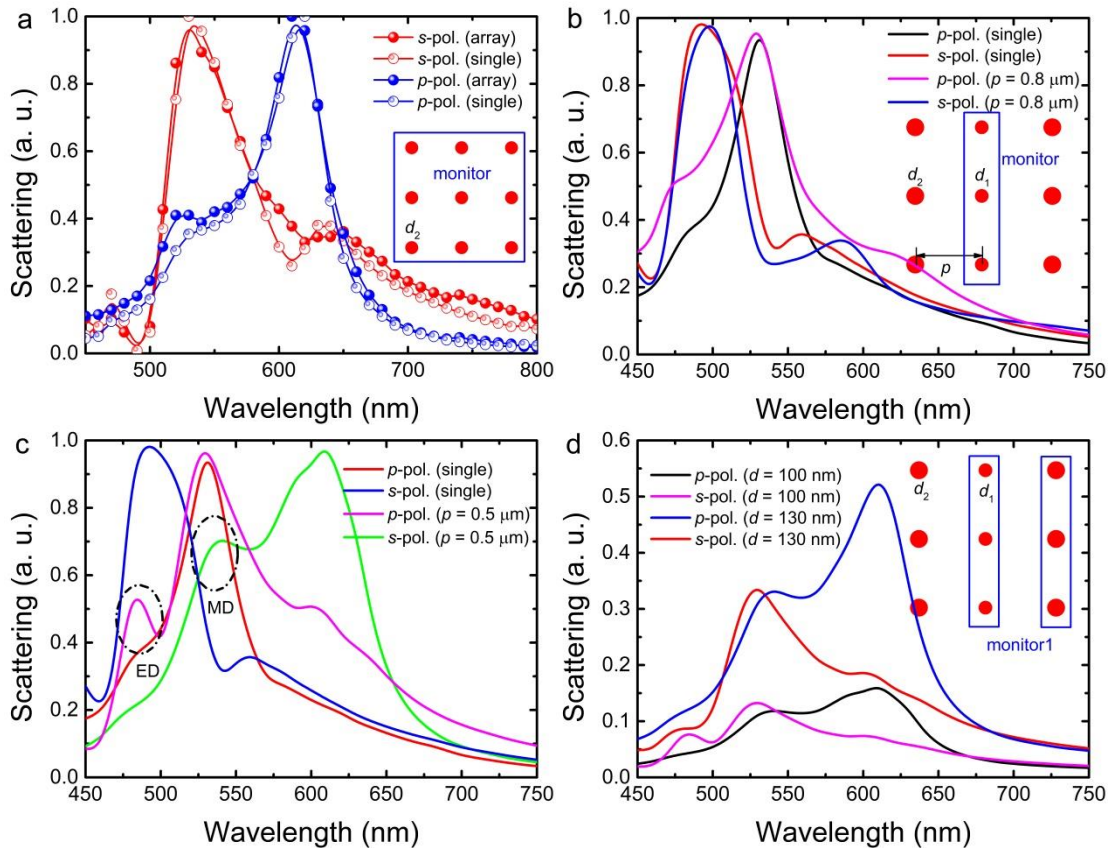

Figure S12: (a) Scattering spectra calculated for a 3×3 array of Si NPs with a period of $p = 500$ nm excited by using *s*- and *p*-polarized light. The scattering spectra calculated for a single Si NP is also provided for comparison. Scattering spectra calculated for a 3×3 array of Si NPs (with different diameters of $d = 100$ and 130 nm) with periods of $p = 500$ nm (b) and $p = 800$ nm (c) excited by using *s*- and *p*-polarized light. The scattering spectra

calculated for a single Si NP is also provided for comparison. (d) Scattering spectra calculated for 3×3 array of Si NPs (d = 100 nm and d = 130 nm) with a period of p = 500 nm excited by using s- and p-polarized light.